Structures of N-terminally processed KRAS provide insight into the role of N-acetylation

Srisathiyanarayanan Dharmaiah[‡], Timothy H. Tran[‡], Simon Messing[‡], Constance Agamasu[‡], William K. Gillette[‡], Wupeng Yan[‡], Timothy Waybright[‡], Patrick Alexander[‡], Dominic Esposito[‡], Dwight V. Nissley[‡], Frank McCormick[‡, §], Andrew G. Stephen[‡], and Dhirendra K. Simanshu[‡,*]

[‡]NCI RAS Initiative, Cancer Research Technology Program, Frederick National Laboratory for Cancer Research, Leidos Biomedical Research, Inc., Frederick, MD 21701, [§]Diller Family Comprehensive Cancer Center, University of California, San Francisco, CA 94158

Supplementary Information

- Supplementary Table 1- 2
- Supplementary Figures 1- 8

Supplementary Table 1: Crystallization conditions for KRAS structures described in this study.

KRAS structures	Crystallization condition
Mg^{2+}-free KRAS (2-169)-GDP	0.056 M $NaPO_4.H_2O$, 1.344 M K_2PO_4, pH 8.2
Mg^{2+}-bound KRAS (1-169)-GDP (P3)	0.2 M $Mg^{2+}Cl_2$, 0.1 M TRIS HCl pH 8.5, 30% PEG 4K
Mg^{2+}-bound KRAS (1-169)-GDP (C2)	6% 2-Propanol, 0.1 M $NaOAc_3H_2O$ pH 4.5, 26% PEG MME 550
Mg^{2+}-free KRAS (2-166)-GMPPNP	200 mM Ammonium Fluoride, 20% PEG 3350
Mg^{2+} bound N-acetylated KRAS (2-169)-GDP	10% w/v PEG 20 000, 20% v/v PEG MME 550, 0.1 M MES/imidazole pH 6.5, 0.02 M of each amino acid (L-Na-Glutamate; Alanine (racemic); Glycine; Lysine HCl (racemic); Serine (racemic))

Supplementary Table 2. Data collection and refinement statistics.

	Mg^{2+}-free KRAS (2-169)-GDP	Mg^{2+}-bound KRAS (1-169)-GDP (P3)	Mg^{2+}-bound KRAS (1-169)-GDP (C2)	Mg^{2+}-free KRAS (2-166)-GMPPNP	Mg^{2+}-bound N-acetylated KRAS (2-169)-GDP
Data Collection					
Resolution range (Å)	42.95 - 1.5 (1.55 - 1.5)	41.92 - 1.45 (1.50 - 1.45)	19.47 - 1.45 (1.5 - 1.45)	35.45 - 1.35 (1.39 - 1.35)	37.23-1.01 (1.05-1.01)
Space group	P 3 2_1	P 3	C 1 2 1	P 2_1 2_1 2_1	C 1 2 1
Unit cell a, b, c (Å) α, ß, γ (°)	77.86, 77.86, 55.73 90, 90, 120	84.18, 84.18, 41.92 90 90 120	66.29, 41.55, 115.38 90, 105.05, 90	36.02, 37.91, 99.99 90, 90, 90	65.19, 41.57, 115.41 90 104.58 90
Total reflections	226355 (22073)	161902 (16251)	185909 (18425)	208763 (19052)	865278 (25971)
Unique reflections	31532 (3103)	58439 (5924)	52619 (5182)	30423 (2915)	148832 (11112)
Multiplicity	7.2 (7.1)	2.8 (2.8)	3.5 (3.6)	6.9 (6.5)	5.8 (2.3)
Completeness (%)	99.77 (99.65)	99.29 (100.0)	96.94 (96.32)	98.37 (95.82)	95.28 (71.39)
Mean I/sigma(I)	18.71 (2.29)	8.73 (1.88)	11.72 (2.27)	24.53 (6.84)	14.84 (1.02)
Wilson B-factor ($Å^2$)	17.25	13.40	14.52	8.99	9.68
R-merge	0.059 (0.678)	0.070 (0.46)	0.056 (0.510)	0.0481 (0.255)	0.0559 (0.6361)
R-meas	0.065 (0.731)	0.087 (0.572)	0.066 (0.602)	0.0521 (0.277)	0.0609 (0.7961)
CC1/2	0.999 (0.847)	0.993 (0.724)	0.998 (0.858)	1 (0.99)	1 (0.904)
Refinement					
Reflections used in refinement	31532 (3101)	58509 (5924)	52618 (5176)	30423 (2913)	148832 (11100)
Reflections used for R-free	2006 (202)	2964 (316)	2007 (200)	1519 (142)	1996 (153)
R-work	0.144 (0.214)	0.134 (0.187)	0.177 (0.245)	0.135 (0.160)	0.1445 (0.3575)
R-free	0.186 (0.289)	0.182 (0.240)	0.216 (0.299)	0.184 (0.209)	0.1663 (0.3748)
CC (work)	0.97 (0.93)	0.59 (0.16)	0.97 (0.90)	0.97 (0.94)	0.974 (0.797)
CC (free)	0.96 (0.89)	0.57 (0.19)	0.96 (0.85)	0.96 (0.90)	0.970 (0.709)
Number of non-H atoms	1729	3083	3230	1644	3395
macromolecules	1469	2705	2824	1422	2859
ligands	28	79	58	37	71
solvent	232	299	348	185	465
Protein residues	168	328	340	169	334
RMS (bonds)	0.003	0.003	0.005	0.009	0.007
RMS (angles)	0.68	0.67	0.83	1.05	1.06
Ramachandran favoured (%)	98.80	97.83	99.11	98.80	99.09
Ramachandran allowed (%)	1.20	2.17	0.60	1.20	0.91
Ramachandran outliers (%)	0.00	0.00	0.30	0.00	0.00
Average B-factor ($Å^2$)	25.05	22.35	16.83	12.58	14.73
macromolecules	22.65	21.09	15.46	11.21	12.71
ligands	17.51	17.22	14.47	7.68	13.51
solvent	41.18	35.15	28.34	24.15	27.34

Statistics for the highest-resolution shell are shown in parentheses.

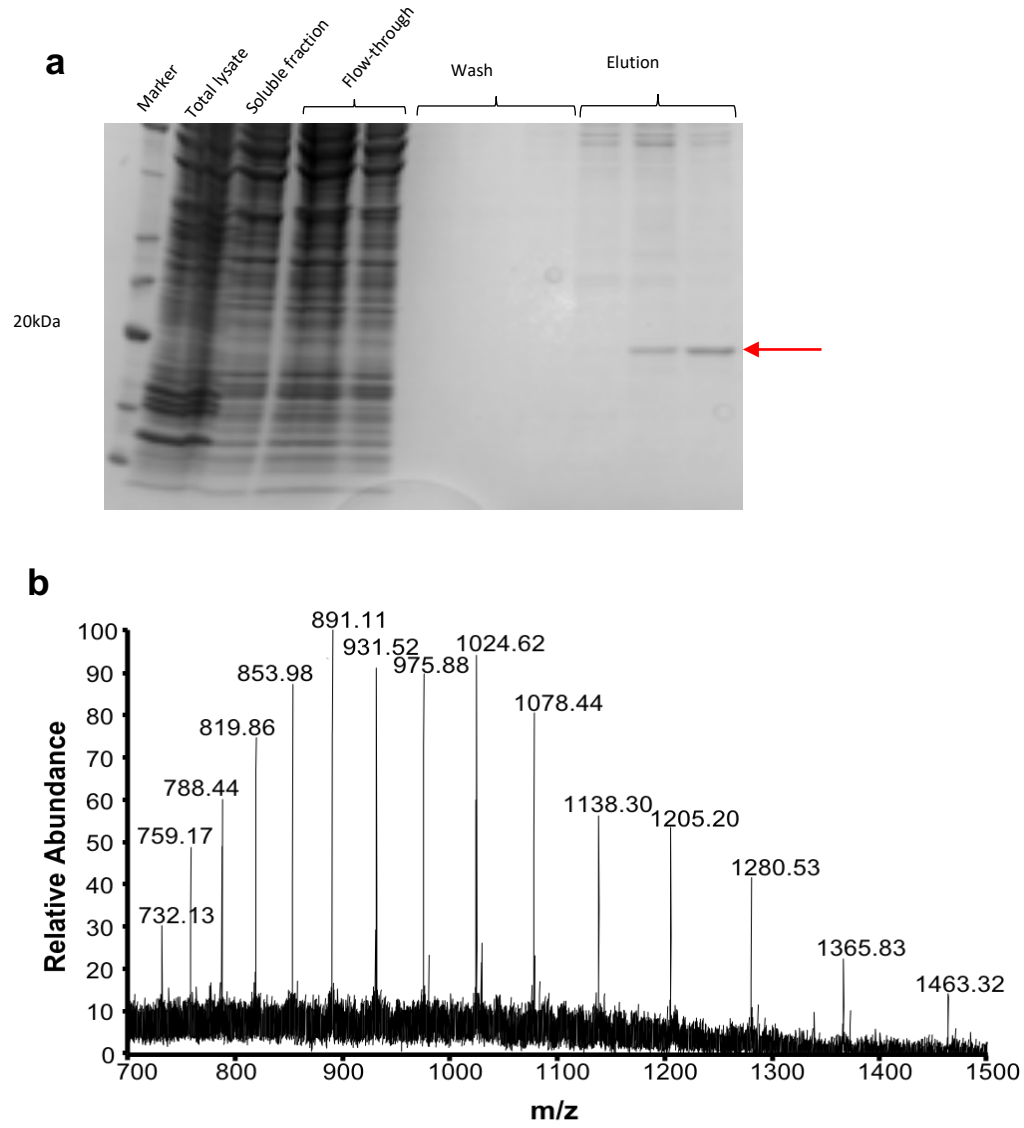

Supplementary Figure 1: Mass spectroscopic characterization of KRAS4b expressed in HEK293 cells. (**a**) SDS-PAGE analysis of human KRAS4b (1-171 with a C-terminal His8 tag) expressed in HEK293 cells and purified using immobilized metal affinity chromatography (IMAC). Red arrow denotes purified KRAS4b. (**b**) The electrospray ionization mass spectrometry (ESI-MS) spectrum of the purified protein is shown. The deconvoluted spectrum is shown in Figure 1.

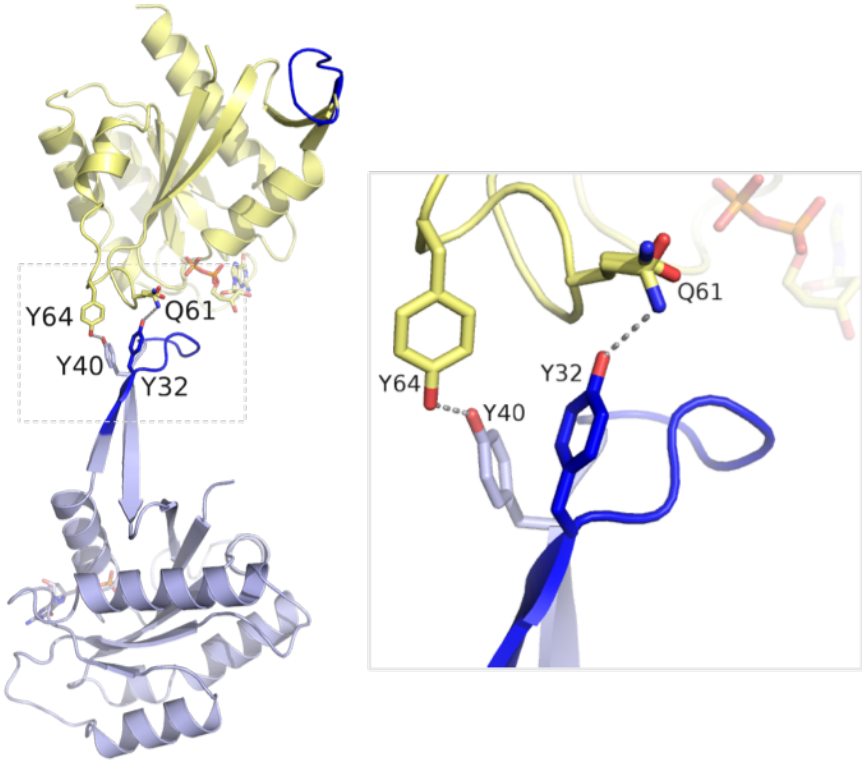

Supplementary Figure 2: Interaction formed by switch I residues in the Mg^{2+}-free KRAS-GDP structure with the residues from the symmetry related KRAS molecule. Residues Y32 and Y40 of Mg^{2+}-free KRAS-GDP (shown in light blue with switch I region highlighted in dark blue) present in the asymmetric unit form H-bonds with Q61 and Y64, respectively, from the symmetry related molecule. Enlarged view of this interaction (shown in box) is shown in the right panel.

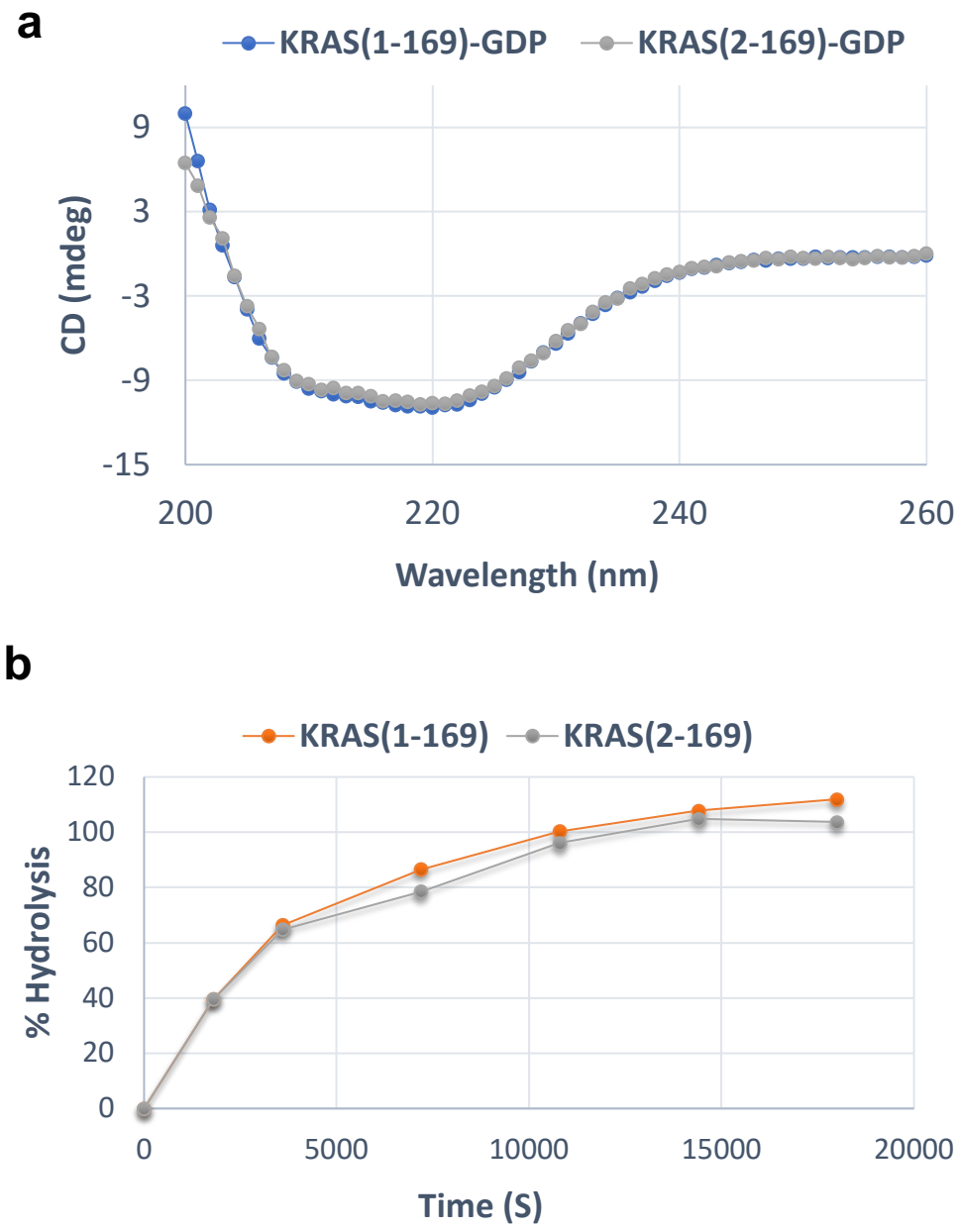

Supplementary Figure 3: Comparison of secondary structural content and rate of intrinsic GTP hydrolysis for KRAS (1-169) and KRAS (2-169). (**a**) Circular dichroism spectra for GDP-bound KRAS (1-169) and KRAS (2-169). (**b**) Plot showing rate of intrinsic GTP hydrolysis for KRAS (1-169) and KRAS (2-169).

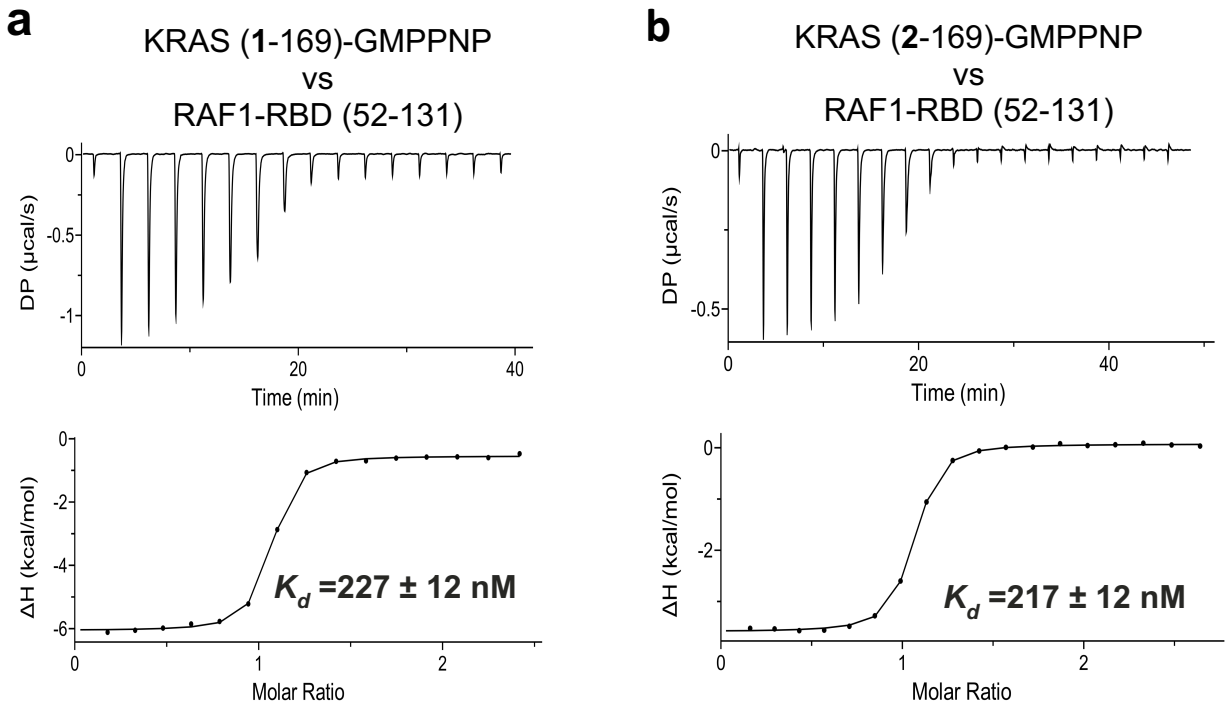

Supplementary Figure 4. Binding affinity of GMPPNP-bound KRAS (1-169) and KRAS (2-169) with RAS-binding domain (RBD) of RAF1. Isothermal titration calorimetry (ITC) experiments to measure the dissociation constant between (**a**) KRAS (1-169)-GMPPNP and RAF1-RBD and between (**b**) KRAS (2-169)-GMPPNP and RAF1-RBD. The DP is a measured differential power between the reference cell and the sample cell.

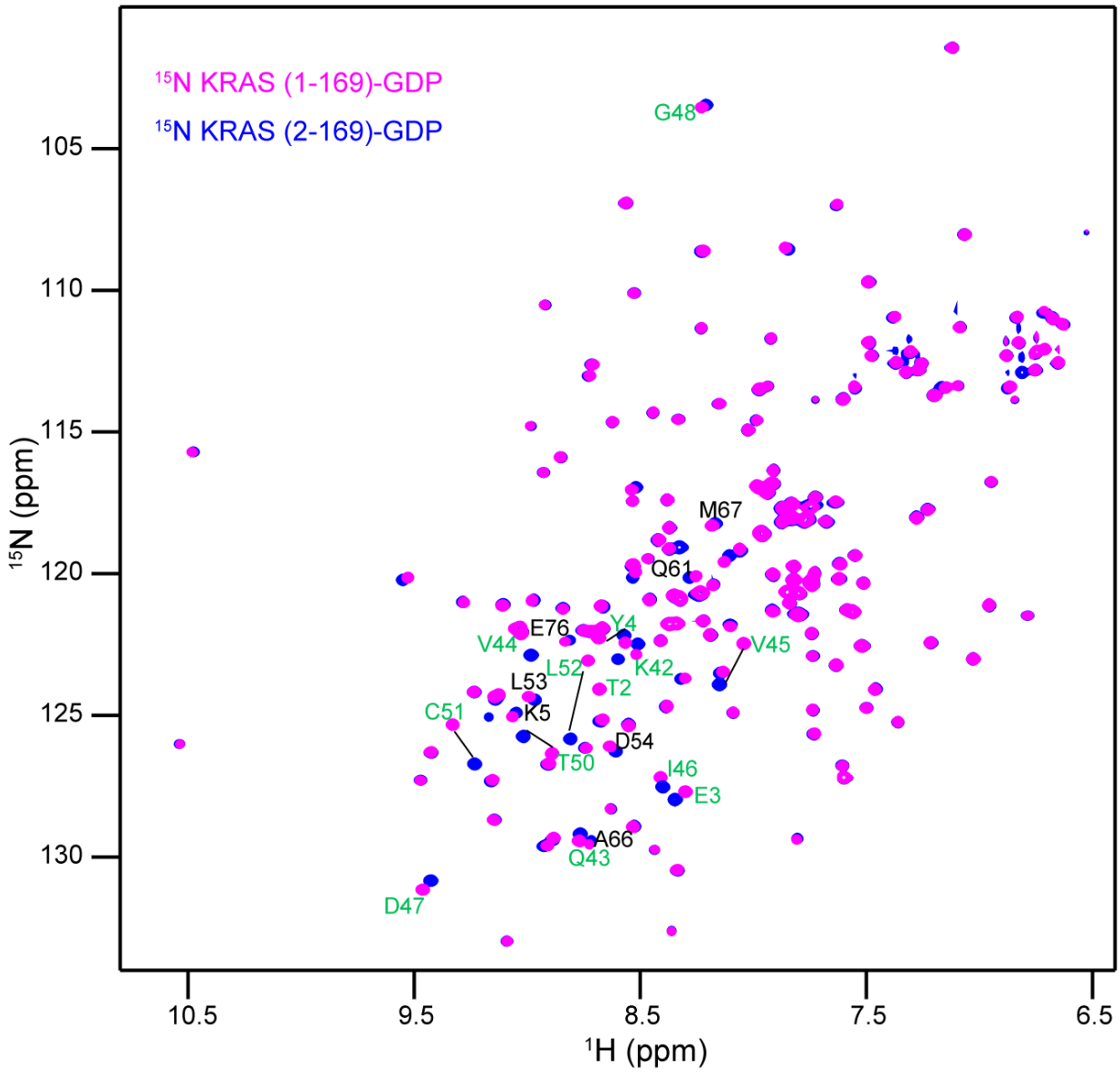

Supplementary Figure 5. Comparison of HSQC spectra obtained for GDP-bound KRAS (2-169) and KRAS (1-169). 2D ^{1}H-^{15}N HSQC spectra obtained for ^{15}N-labeled KRAS (1-169) (magenta) and free ^{15}N labeled KRAS (2-169) (blue). Amide signals that exhibited substantial chemical shift differences are labeled in green.

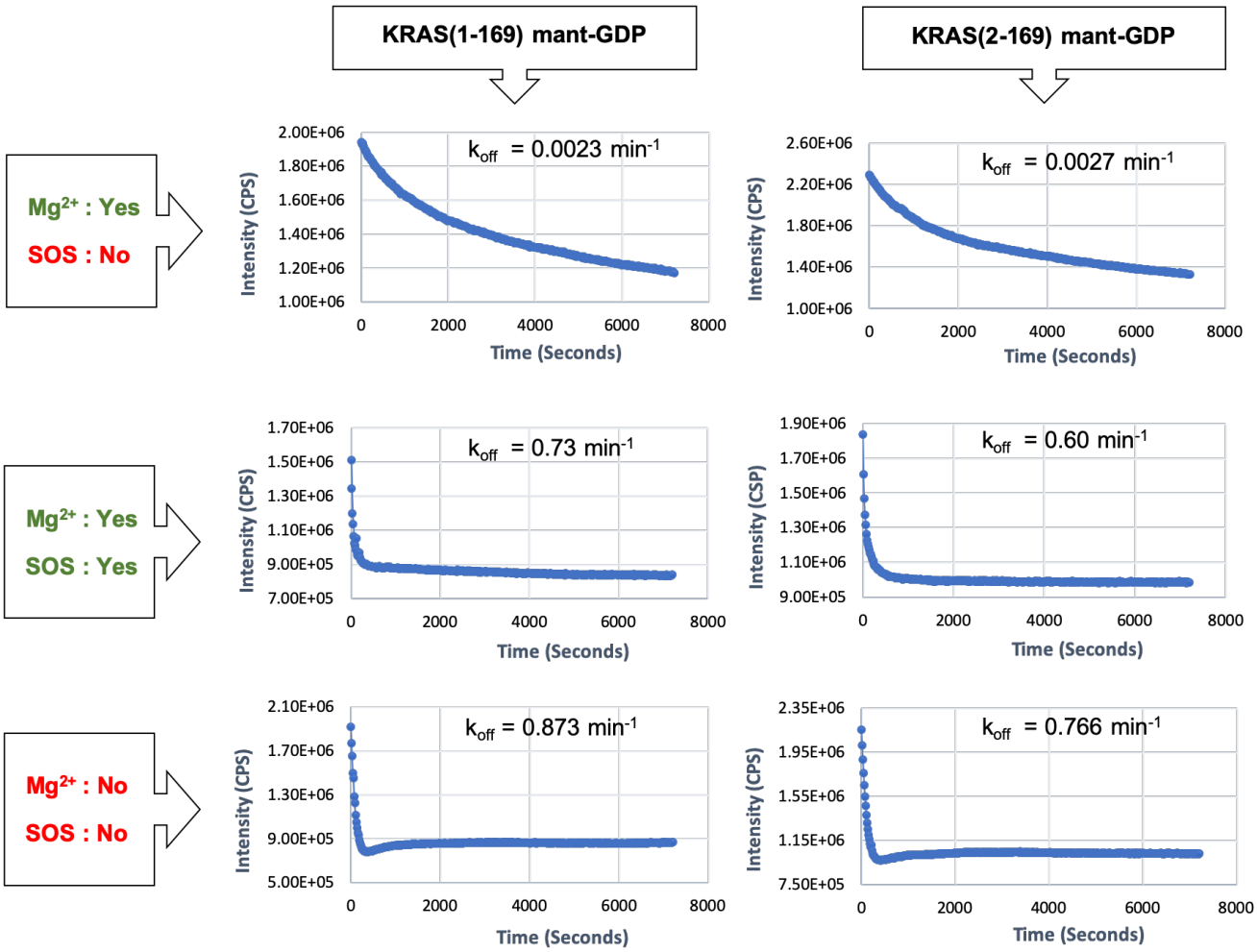

Supplementary Figure 6: Intrinsic and SOS-mediated nucleotide exchange rate for KRAS proteins in the presence and absence of initiator methionine. In the presence of Mg^{2+} in the reaction mixture, both KRAS proteins (1-169 and 2-169) showed similar rates for intrinsic and SOS-mediated nucleotide exchange. However, in the absence of Mg^{2+} in the reaction mixture, both KRAS proteins showed intrinsic exchange rates higher than the SOS-mediated exchange rate obtained in the presence of Mg^{2+}. When SOS was added to this Mg^{2+}-free reaction mixture, the reaction occurred so rapidly that the majority of the nucleotide was displaced before the first measurement was made (data not shown).

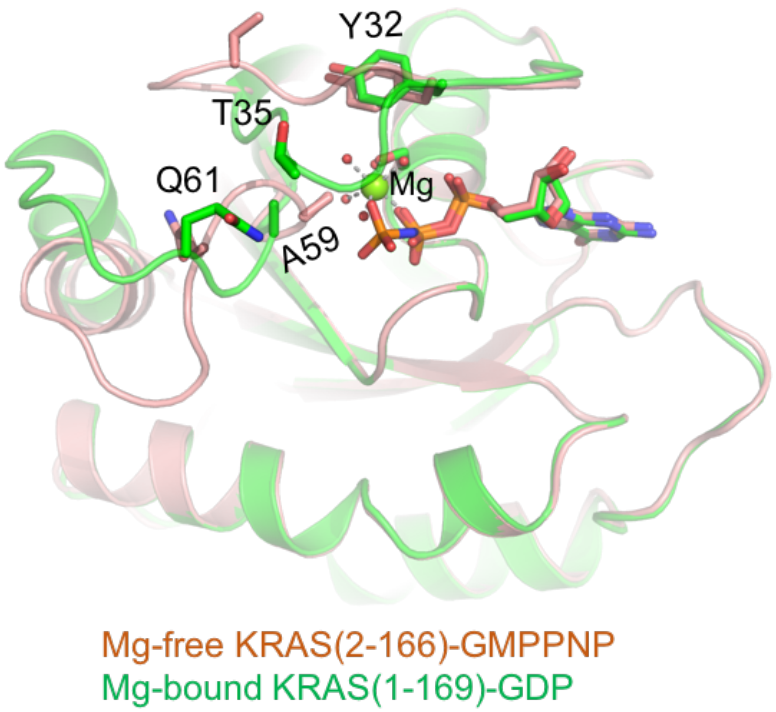

Supplementary Figure 7: Structural superposition of Mg^{2+}-free KRAS (2-166)-GMPPNP with Mg^{2+}-bound KRAS (1-169)-GDP structures. KRAS is shown in ribbon representation, GDP and sidechain atoms of KRAS are shown in stick representation.

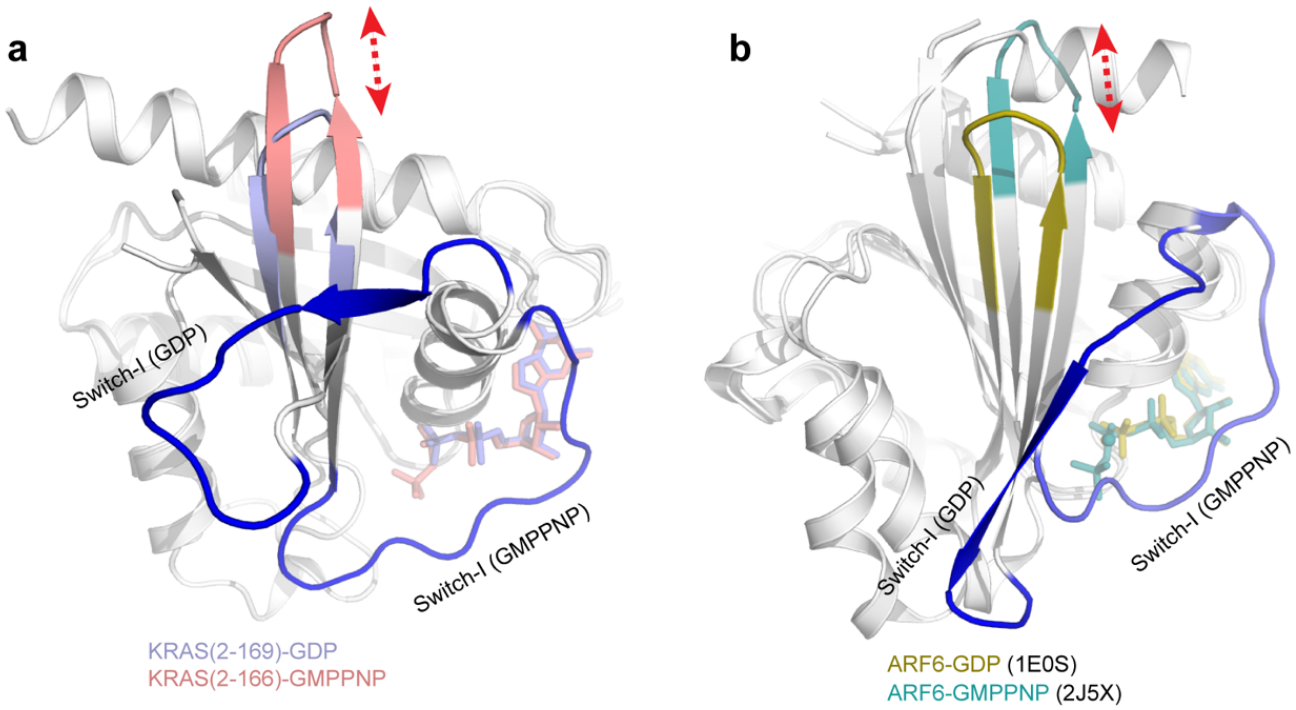

Supplementary Figure 8: Mg^{2+}-free KRAS structures resemble conformational changes seen previously in Mg^{2+}-bound ARF6 structures. Structural superposition of (**a**) Mg^{2+}-free GDP/GMPPNP-bound KRAS structures and (**b**) Mg^{2+}/GDP/GMPPNP-bound ARF6 structures showing presence of additional β-strand in the switch I region as well as conformational changes in the turn between β2 and β3 strands.